Challenges in Numerical Weather Prediction of the 10 August 2020 Midwestern Derecho: Examples from the FV3-LAM

by

William A. Gallus, Jr[1]. and Michell A. Harrold[2]

[1]*Department of Geological and Atmospheric Sciences, Iowa State University, Ames, IA*

[2]*Developmental Testbed Center, National Center for Atmospheric Research/Research Applications Laboratory and Developmental Testbed Center, Boulder, CO*

Revision submitted to *Weather and Forecasting* on 25 May 2023

Corresponding Author Address: William A. Gallus, Jr., 3025 Agronomy Building, 716 Farm House Lane, Ames, IA, 50011, wgallus@iastate.edu

ABSTRACT

A severe derecho impacted the Midwestern United States on 10 August 2020, causing over 12 billion dollars in damage, and producing peak winds estimated at 63 m s^{-1}, with the worst impacts in Iowa. The event was not forecast well by operational forecasters, nor even by operational and quasi-operational convection-allowing models.

In the present study, nine simulations are performed using the Limited Area Model version of the Finite-Volume-Cubed-Sphere model (FV3-LAM) with three horizontal grid spacings and two physics suites. In addition, when a prototype of the Rapid Refresh Forecast System (RRFS) physics is used, sensitivity tests are performed to examine the impact of using the Grell-Freitas (GF) convective scheme.

Several unusual results are obtained. With both the RRFS (not using GF) and Global Forecast System (GFS) physics suites, simulations using relatively coarse 13 and 25 km horizontal grid spacing do a much better job of showing an organized convective system in Iowa during the daylight hours of 10 August than the 3-km grid spacing runs. In addition, the RRFS run with 25-km grid spacing becomes much worse when the GF convective scheme is used. The 3-km RRFS run that does not use the GF scheme develops spurious nocturnal convection the night before the derecho, removing instability and preventing the derecho from being simulated at all. When GF is used, the spurious storms are removed and an excellent forecast is obtained with an intense bowing echo, exceptionally strong cold pool, and roughly 50 m s^{-1} surface wind gusts.

1. Introduction

Derechos, thunderstorm systems that produce an extensive swath of wind damage (Hinrichs 1888; Johns and Hirt 1987), often with at least some reports of significantly severe wind (65 knots or greater, 33.4 m s^{-1}), occur roughly 15 times per year in the United States (Bentley and Mote 1998; Bentley and Sparks 2003). There is disagreement over the specific size criteria needed for these thunderstorm systems to be classified as a derecho (Johns and Hirt 1987; Bentley and Mote 1998; Evans and Doswell 2002; Bentley and Sparks 2003; Coniglio and Stensrud 2004; Coniglio et al. 2014; Corfidi et al. 2016), but all definitions imply potentially damaging winds over a large area (e.g., major axis of 400 km or more) so that large monetary losses, and many injuries and fatalities, are possible (Ashley and Mote 2005). Often, they are produced from one or more bow echoes (Weisman 1993).

At least three mechanisms are believed to contribute to the strong winds in derechos: a descending rear inflow jet, downbursts, and mesovortices. Descending rear inflow jets (e.g., Rutledge et al. 1988; Weisman 1992) were shown in Mahoney and Lackmann (2011) to be more likely to cause severe surface winds when the environment was drier at midlevels, favoring more evaporative cooling and downward motion. Downbursts (Fujita 1978) likewise may be formed by dry air and evaporative cooling but can also be present in moister environments where latent cooling from melting of frozen hydrometeors may be strong. Mesovortices, which develop from tilting of horizontal vorticity into the vertical and stretching of vorticity, can produce narrow swaths of enhanced winds (e.g., Weisman and Trapp 2003; Trapp and Weisman 2003; Atkins and Laurent 2009).

Because these mechanisms can explain the strong winds observed in derechos, derechos can happen in a range of synoptic environments (e.g., Cohen et al. 2007). Johns and Hirt (1987) originally classified derechos as being serial or progressive. Progressive derechos often occur near or just north of a warm or stationary front or other boundary and tend to move more quickly than the serial ones, and often faster than the mean flow. Serial derechos are more likely ahead of cold fronts. Doswell and Evans (2003) classified derechos as existing with strong forcing, weak forcing, and a hybrid mixture. They found strong forcing derechos existed in environments with relatively strong low-level winds and wind shear, whereas weak forcing events happened with relatively weak vertical wind shear but large CAPE. Strongly forced events generally had cooler, less unstable conditions present. Strong forcing would likely be present for most serial derechos, with weak forcing more common for progressive ones. Doswell and Evans (2003) found that it was difficult to predict when derechos would occur as compared to supercells, because the environments often share similar characteristics. Cohen et al. (2007) examined differences in MCS environments not associated with severe wind, those that were, and those associated with derechos. They found deep layer shear had greater predictive skill than shear present in layers closer to the ground to distinguish derecho-producing MCSs, but CAPE did not differentiate well.

Although the environments that favor derechos are well known, prediction of individual events remains difficult (e.g., Gallus et al. 2005; Grunzke and Evans 2017; Ribeiro et al. 2022). The evolution of thunderstorms that organize into a derecho can be complex. It is likely the intensity and upscale evolution of a cold pool plays a substantial role, and these are sensitive to both small-scale dry layers that may not be well-resolved by the rawinsonde network, and how the convective updrafts themselves evolve and grow upscale. The convective updraft organization influences the development of potentially strong mesoscale convective vortices that facilitate production of severe winds over large spatial regions and long time periods. The 4 June 1999 derecho studied in Gallus et al. (2005) is a good example of a poorly predicted event where deficiencies in the ability of the observing network to resolve small scale weather features likely prevented models from simulating the convective system that produced the derecho. On the other hand, the 8 May 2009 derecho, which produced many gusts of greater than 35 m s^{-1} with isolated 45 m s^{-1} gusts as it traveled from western Kansas to eastern Kentucky (Coniglio et al. 2011), was reasonably simulated by some models (Weisman et al. 2013), despite occurring in an environment that was not "synoptically-evident", as the thunderstorms were not forced by a synoptic-scale weather system with easily identifiable fronts or boundaries (Coniglio et al. 2011).

An even more intense progressive derecho that was not well-predicted by numerical models and operational forecasters occurred in the Midwestern United States on 10 August 2020. Because winds over 45 m s^{-1} affected numerous agricultural counties in this region, flattening millions of acres of corn, total damages exceeded 12 billion dollars (NCEI 2022). The present study examines nine simulations of the Limited Area Model (LAM) version of the Finite-Volume-Cubed-Sphere atmospheric dynamical core (FV3-LAM; Black et al. 2021) of this progressive derecho to gain insight into why the event may have been so poorly predicted. The FV3 dynamical core has already been implemented into the operational Global Forecast System (GFS) model at the National

Centers for Environmental Prediction (NCEP) and has been chosen to be the dynamical core used within NOAA's Unified Forecasting System (UFS)-based operational modeling suite. The UFS includes model applications from global down to regional domains, including seasonal to sub-hourly timescales, and as such, it is imperative that it can provide accurate forecasts for a wide spectrum of meteorological phenomena as well as routine and high impact weather events. Therefore, as the LAM version of the UFS prepares to become operational, it is important to investigate how the UFS Short-Range Weather (SRW) application handles extreme events such as this one. The simulations are performed with three horizontal grid spacings and two physics suites, and sensitivity tests are performed to explore the role of the convective parameterization in one of the suites. A key question being addressed by this study is: Can the different physics suites represent the high-impact derecho at varying grid spacings? Traditionally, the GFS has been developed, run, and tested at ~25-km and ~13-km horizontal grid spacings (i.e., global scales), while the RRFS (Rapid Refresh Forecast System) has focused on convective-allowing scales (~3-km horizontal grid spacing). As the UFS moves toward model unification, it is important to understand the abilities of different physics suites to perform at different grid lengths.

2. Data and Methodology

FV3-LAM runs were initialized using 0000 UTC 10 August 2020 hourly output from the experimental version of the High-Resolution Rapid Refresh (HRRRx) model (Benjamin et al. 2009; 2011; 2013; Dowell et al. 2022; James et al. 2022) running during summer 2020, later known as HRRRv4. This limited area version of the FV3 model (Harris and Lin 2013, 2014; Lin 2004; Putman and Lin 2007) was developed from the same FV3 model version that began running operationally in the NCEP GFS model in June 2019 (see Black et al. 2021 for details of the FV3-LAM) and is being rapidly developed. The experimental HRRR model was used to provide the initial conditions (ICs) and lateral boundary conditions (LBCs) since it was one of the few quasi-operational or operational convection-allowing models (CAMs) initialized at 0000 UTC 10 August to show an organized convective system with a hint of a bow echo structure in its simulated reflectivity across Iowa during the daylight hours of 10 August when the derecho was moving across that region.

The FV3-LAM was run over a continental United States domain with three horizonal grid spacings (25, 13, and 3 km), as the 2020 derecho event was one of several cases being used to test the scale-awareness of two physics suites available in the Common Community Physics Package (CCPP) (Heinzeller et al. 2023). All simulations used 66 vertical layers and were integrated for 24 hours. The two physics suites used in the model represented roughly what was used in two operational models, the GFS and HRRR, during 2020. The GFSv16 beta physics suite (GFS hereafter) that was used consisted of the following parameterizations: the Geophysical Fluid Dynamics Laboratory microphysics (Zhou et al. 2019), the hybrid eddy-diffusivity mass-flux planetary boundary layer scheme (Han et al. 2016), the GFS surface layer scheme (Long 1986, 1989), the Rapid Radiative Transfer Model (Iacono et al. 2008; Mlawer et al. 1997) for both shortwave and longwave radiation, the scale-aware Simplified Arakawa-Schubert (SAS) convection scheme (Han et al. 2017), and the Noah land surface model (LSM; Ek et al. 2003). The version of the physics suite similar to that used in the HRRR in 2020, the Rapid Refresh Forecast System beta version 1 (hereafter RRFS), consisted of the Thompson-Eidhammer (2014) microphysics, MYNN-EDMF (Mellor-Yamada-Nakanishi-Niino Eddy Diffusivity/Mass Flux) planetary boundary layer (Nakanishi and Niino 2009, Olson et al. 2019) and MYNN (Mellor-Yamada-Nakanishi-Niino) surface (Olson et al. 2021) schemes, the Grell-Freitas (2014) (GF) convective scheme, and the GFS NoahMP LSM (Niu et al. 2011). The GF scheme consists of separate parameterizations for deep convection and for shallow convection, but the two are typically run together as in the present study. For the RRFS runs, an additional set of simulations was performed where the GF convective scheme was turned off, since NOAA plans to replace the HRRR and RAP (Rapid Refresh) models with the FV3-LAM using the RRFS physics suite in the future, and questions remain about any need for the GF scheme to be used with CAM grid spacings. There are no plans to run the SAS scheme from the GFS suite with CAM grid spacings, and thus no tests were performed in the present study where SAS was not used with that suite. The nine configurations used are summarized in Table 1.

Physics Suite	Horizontal Grid Spacing (km)	Convective Scheme
RRFS	25	GF
RRFS	25	none
RRFS	13	GF
RRFS	13	none
RRFS	3	GF
RRFS	3	none
GFS	25	SAS
GFS	13	SAS
GFS	3	SAS

Table 1: Summary of the nine simulations performed in the present study.

3. Overview of the 10 August 2020 Derecho

The convective system that produced the Midwestern derecho of 10 August 2020 initiated between 0700 - 0900 UTC as elevated thunderstorms over south-central South Dakota that grew upscale as the system moved southeastward. Significant severe wind gusts (over 33 m s^{-1}) began just before 1400 UTC (Fig. 1a). The initial convection formed behind a cold front that was located over northeast Nebraska and the far northwest tip of Iowa at 0900 UTC, and then crossed the front and moved into much more unstable air, becoming surface based by 1600 UTC (Fig. 1b). Convection then intensified as it moved primarily eastward, reaching the Cedar Rapids, IA area around 1800 UTC (Fig. 1c). This is the where the peak estimated wind gust occurred, along with measured winds as strong as 56 m s^{-1}. The system remained intense as it moved eastward into Illinois, although the peak straight-line winds decreased while the number of tornadoes increased as it neared Lake Michigan after 2000 UTC (Fig. 1d). Around this time, the line of thunderstorms was developing much more rapidly to the south, extending well into Missouri. The distribution of storm reports for the main portion of the event can be seen in Fig. 2 (a few reports occurred before 1200 UTC with the first as early as 1016 UTC in southern South Dakota). The system continued to produce severe winds and wind damage until around 0200 UTC 11 August 2020 when it was in western Ohio, having traveled over 1200 km in about 14 hours.

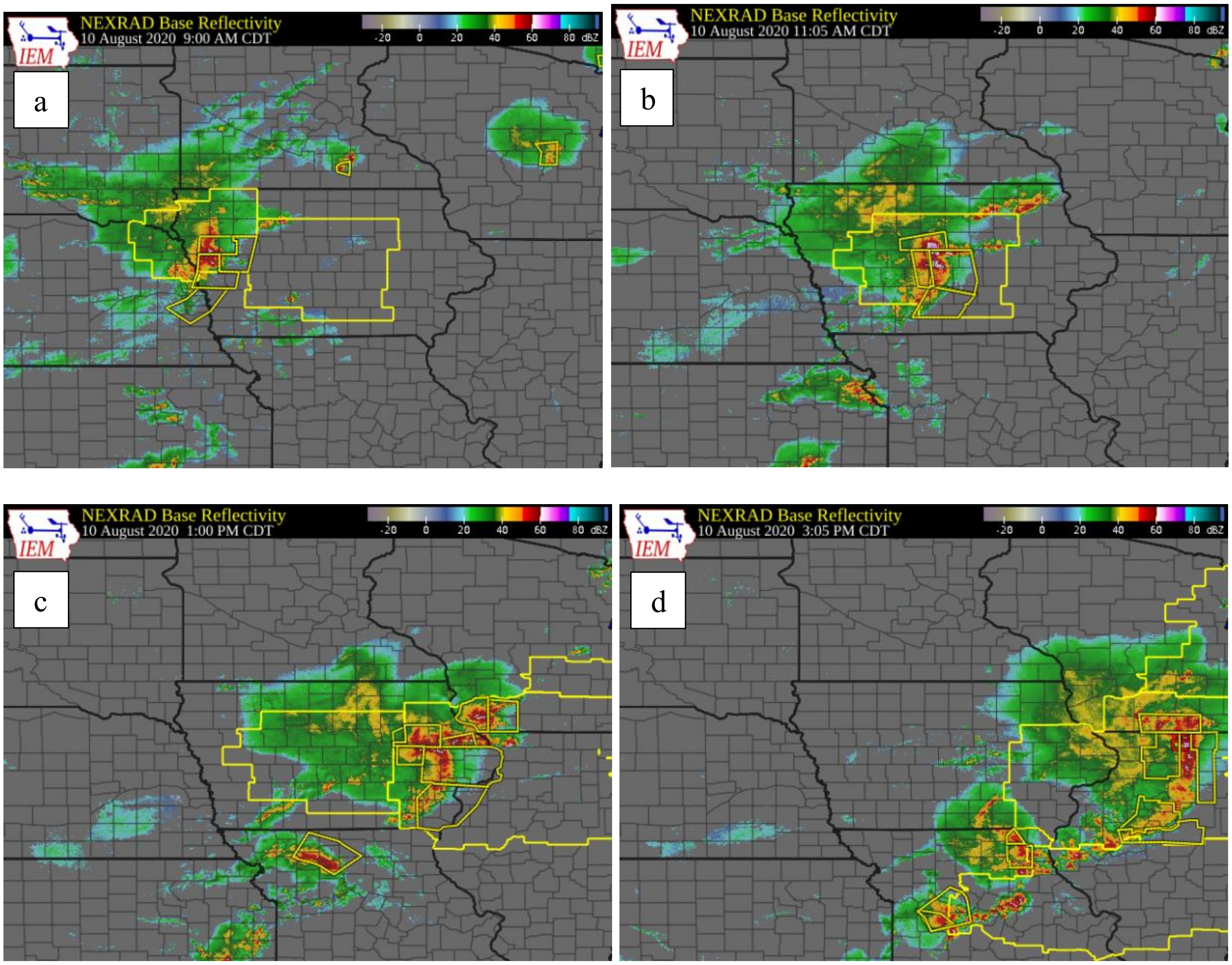

Figure 1: Composite NEXRAD reflectivity at a) 1400, b) 1600, c) 1800, and d) 2000 UTC on 10 August 2020. Severe thunderstorm warnings are overlaid with thin yellow lines. Severe thunderstorm watches are indicated with thicker yellow lines. The images are from the Iowa Environmental Mesonet.

Despite the convective system being very well-organized, it was not well-predicted, at least more than a few hours before it occurred. Storm Prediction Center Day 2 severe weather outlooks issued less than 24 hours before the extensive wind damage began (Fig. 3a) indicated only a 5-15% probability of severe thunderstorm winds in the region impacted by the derecho in far eastern and southern Iowa, with no risk indicated in central Iowa where significant damage also occurred. Issued even less than 12 hours before the event began, the 0600 UTC Day 1 update still only indicated a 5-15% probability for severe thunderstorm winds (Fig 3b) over a slightly larger portion of the part of Iowa later impacted by the derecho.

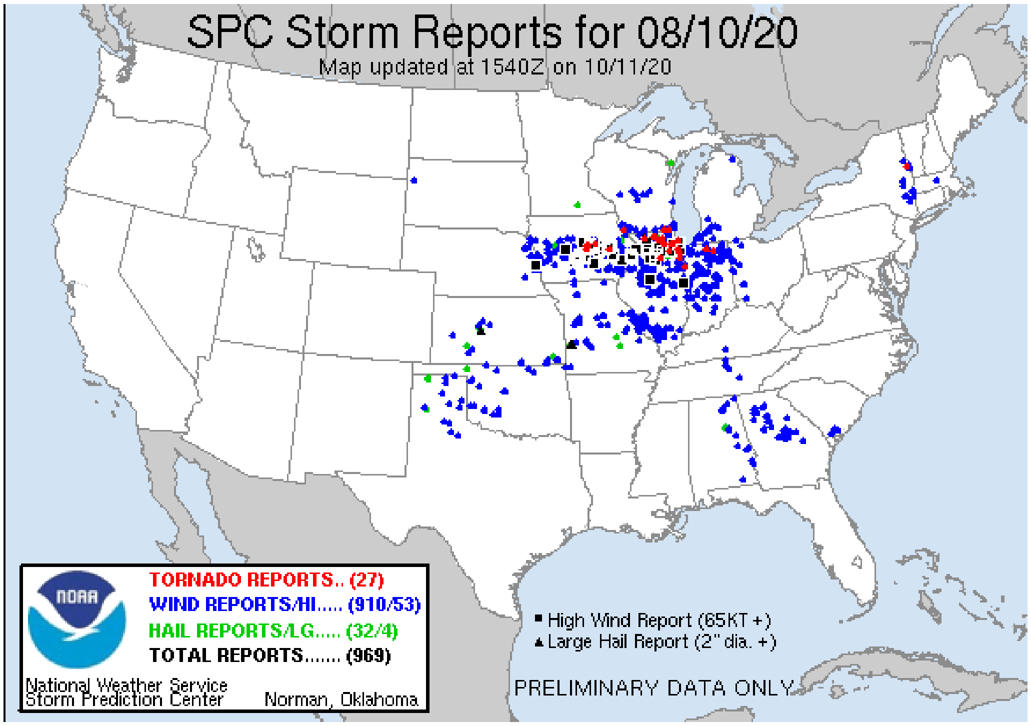

Figure 2: Storm reports received at the SPC as of 11 October 2020 for the period 1200 UTC 10 August – 1200 UTC 11 August 2020. Blue dots represent severe thunderstorm wind reports (winds of 50 kts or more), with black squares identifying significant severe reports (> 65 kts).

The SPC forecasts reflected the operational numerical model guidance at the time which showed a cold front to have moved across much of Iowa by the morning of 10 August, with convection in the state during the daylight hours of 10 August being elevated and displaced across northern Iowa in runs parameterizing convection, or having already moved out of the state due to spurious initiation the previous night in most CAMs. An example of the poor CAM forecasts can be seen in Fig. 4, which depicts the simulated reflectivity valid at 1800 UTC from four High Resolution Ensemble Forecast (HREF) members initialized at 0000 UTC 10 August 2020. None of these simulations had an organized convective system in Iowa during the mid-day to afternoon hours, as they all had triggered spurious convection the night before over the state, which had

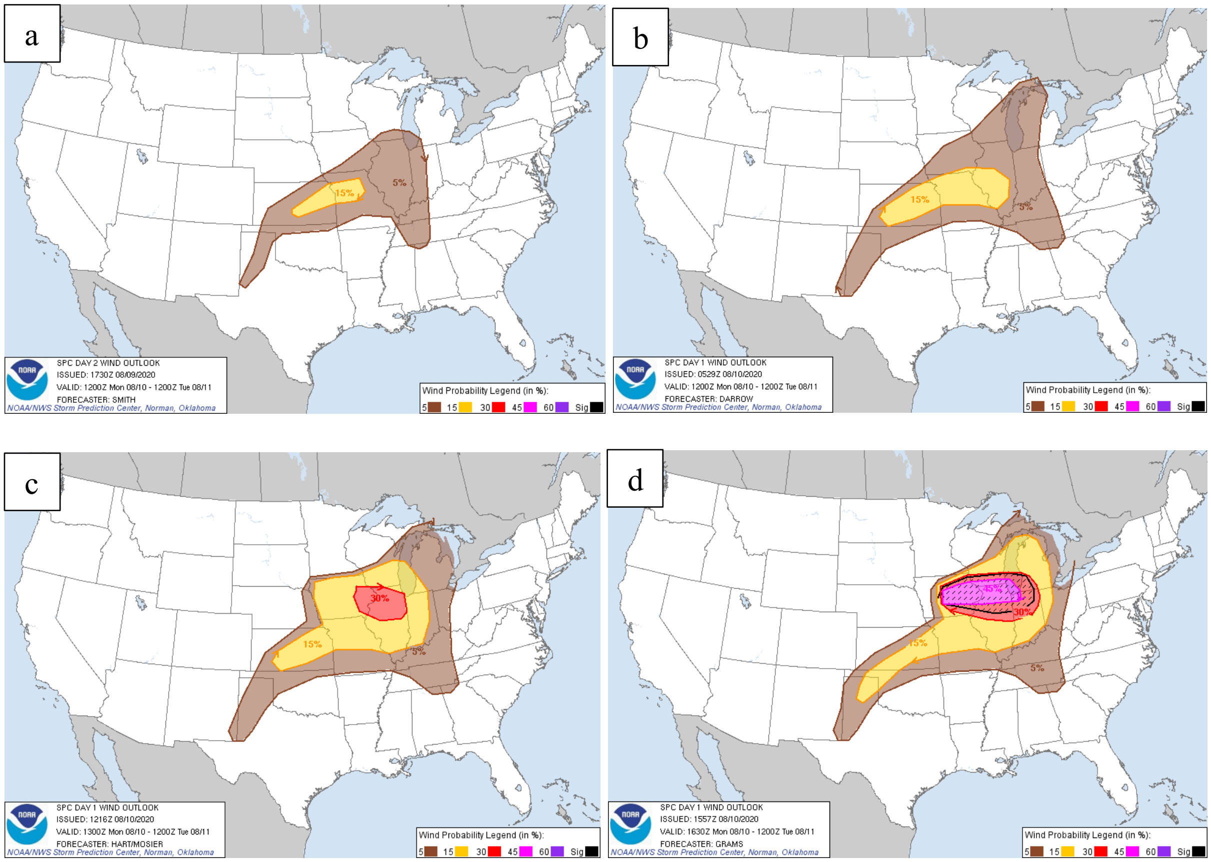

Figure 3: Probabilistic damaging wind forecasts from SPC convective outlooks issued at a) 1730 UTC 9 August 2020 (Day 2 update), and b) 0600 UTC, c) 1300 UTC, and d) 1630 UTC 10 August 2020, valid for the period 1200 UTC 10 August – 1200 UTC 11 August 2020.

already moved east or southeast of Iowa by the time the derecho was observed. In all but the Nonhydrostatic Mesoscale Model on B-grid (NMMB), the displacement errors were hundreds of kilometers (compare to Fig. 1c). As might be expected with such poor numerical model guidance, it was not until the 1300 UTC outlook on 10 August 2020 when SPC updated the forecast to indicate a Slight risk over most of the state of Iowa with at least a 15% probability of severe wind over Iowa and over 30% probability in eastern and northern Illinois (Fig. 3c). The 1630 UTC update increased the severe risk once again, with a Moderate risk introduced for all areas east of the current position of the convective system, as far east as northwestern Indiana, with wind probabilities exceeding 45% (Fig. 3d) and a forecast of 10% or greater probabilities for significantly severe wind. Numerous significant severe wind reports had already been received from western and central Iowa by this time.

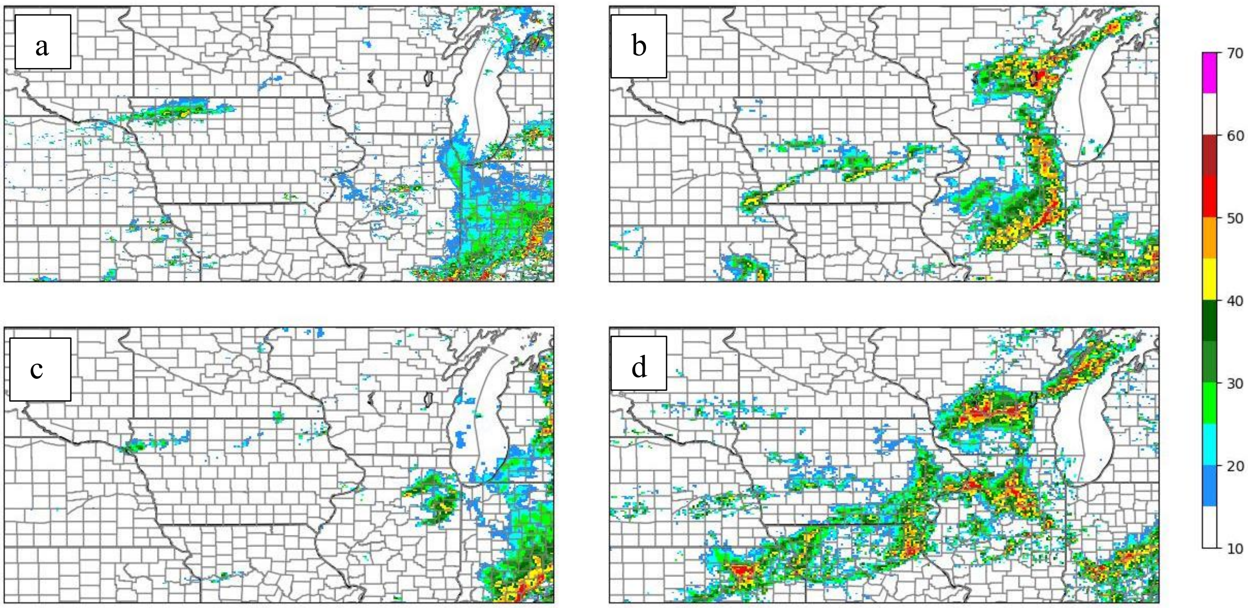

Figure 4: Simulated composite reflectivity valid at 1800 UTC 10 August 2020 from four HREF members initialized at 0000 UTC 10 August 2020, with a) 3-km North American Model Nest (Rogers et al. 2017), b) High Resolution Window Advanced Research Weather Research and Forecasting (WRF) model (Skamarock et al. 2008), c) CONUS Member 2 (formerly known as the National Severe Storms Laboratory WRF; Kain et al. 2010), and d) High Resolution Window NMMB (Janjic and Gall 2012).

4. Results

The FV3-LAM simulations of the 10 August 2020 derecho performed here with different physics suites and grid spacings exhibited some behaviors counter to what is normally expected when grid spacing is refined or a convective scheme is used. The simulated reflectivity at 1800 UTC when the strongest winds were observed in the derecho showed large variations in the runs using RRFS physics, depending on whether the GF scheme was being used (Fig. 5). Reflectivity in the FV3-LAM with RRFS physics is computed not only using hydrometeors from the microphysics scheme, but also using the GF rainfall component, if there are no hydrometeors (G. Grell, NOAA, 2023, personal communication). As an example of the large variations, in the 25-km runs, the run without GF correctly showed intense echo in central Iowa (Fig. 5a), although the coarseness of the grid prevented realistic bowing structure from being simulated. The 25-km run

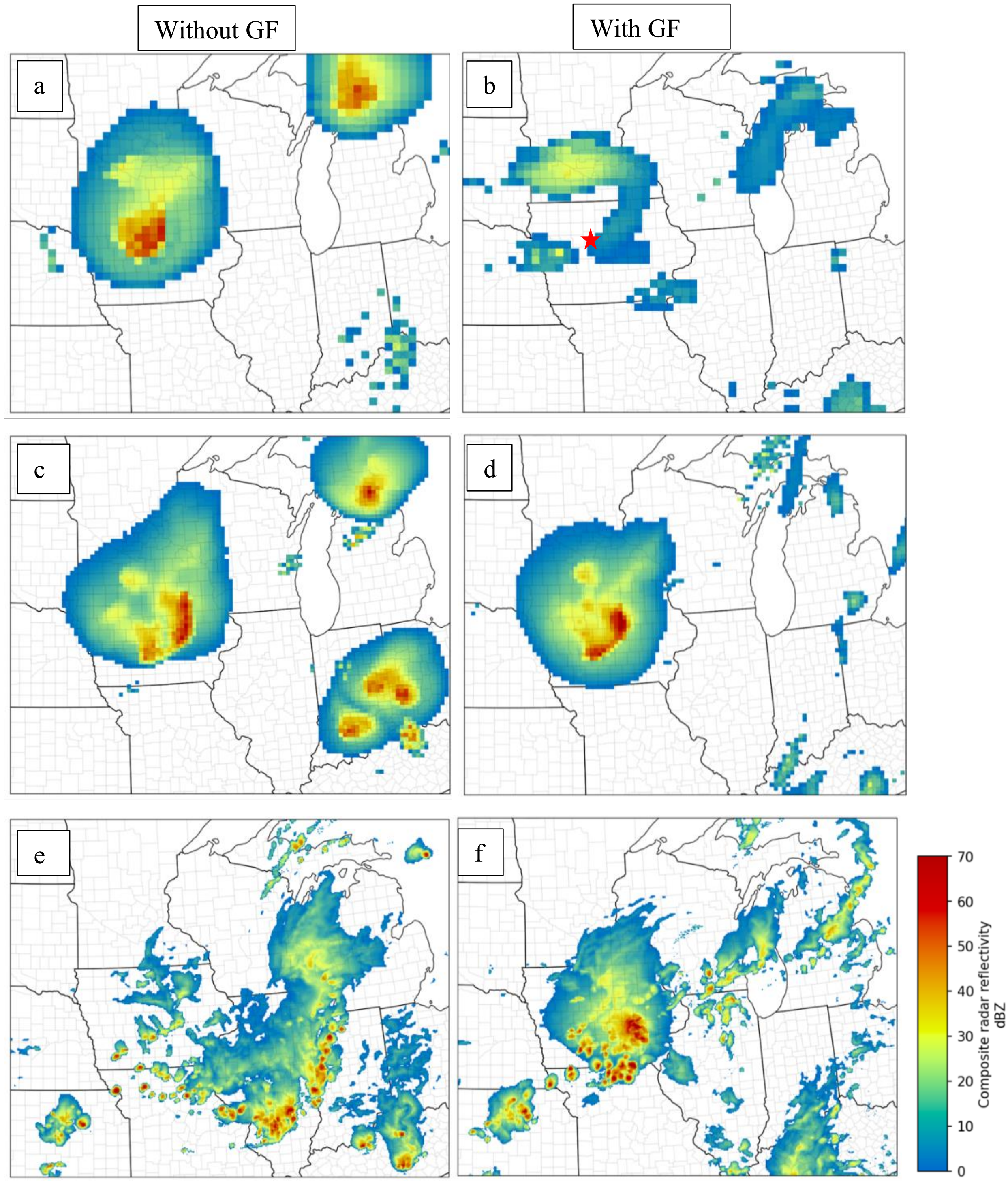

Figure 5: Simulated reflectivity (see color bar at right) at 1800 UTC for the RRFS runs initialized at 0000 UTC 10 August 2020 for a) 25 km without GF, b) 25 km with GF, c) 13 km without GF, d) 13 km with GF, e) 3 km without GF, and f) 3 km with GF. The observed radar valid at this time can be found in Fig. 1b. Red star in panel b shows where sounding is taken from in Fig. 9.

with GF, however, was not nearly as good (Fig. 5b), with the echo over Iowa being greatly diminished and the main area of reflectivity being weaker and pushed north into southern Minnesota.

The negative impact of the use of the GF scheme in the 25-km run can also be seen in the total precipitation during the 24 hours ending at 0000 UTC 11 August 2023 (Fig. 6). The 25-km simulation with GF (Fig. 6b) lacked the intense system in Iowa that had been simulated in four other runs: the 25-km run that did not use GF (Fig. 6a), both 13-km runs (Fig. 6d, e), and the 3-km run that used GF (Fig. 6h). In fact, an analysis of total hourly precipitation (including both grid-resolved and that from the GF scheme) during the period from 1500-1800 UTC (not shown) indicated no precipitation in the part of northern Iowa that does not have reflectivity (Fig. 5b) in the 25-km run with GF, so this much worse simulated radar depiction was not due to GF-produced precipitation reducing simulated reflectivity. Instead, the reasons for the substantial difference appear to be related to (i) the formation of light precipitation from the GF scheme that extended eastward roughly 100 km more into the warm sector (Fig. 7b) from where precipitation occurred in the run without GF (Fig. 7a), which kept the lower troposphere cooler than in the run without GF by mid-morning through midday (see Fig. 8 for 1400 UTC), and (ii) the formation of a stronger cold pool (Fig. 8) under the much stronger convection near the northwest tip of Iowa in the run without GF by 1400 UTC (Fig. 7a), which did not exist in the run with GF (Fig. 7b). The more intense convection in the run without GF, which came from upscale growth of convection moving generally eastward into Iowa from southeastern SD and northeastern NE, similar to that observed and that present in the 13 km horizontal grid spacing runs and the 3 km run that did use GF, allowed the formation of a strong enough cold pool to encourage lift ahead of it as it moved into the more capped airmass over central Iowa. This lift created a moist absolutely unstable layer (Bryan and Fritsch 2000) by 1700 UTC (Fig. 9) in the 650-400 hPa layer associated with the intense elevated convection seen at 1800 UTC in Fig. 5a. In addition, the most unstable CAPE was much greater in the run without GF, 4423 J kg^{-1} compared to 3215 J kg^{-1} in the run with GF. The most unstable CIN, however, did not change much, with -31.6 J kg^{-1} when GF was not used, and -39.4 J kg^{-1} when GF was used. The intense convection that formed in the run without GF resulted in the formation of a strong midlevel mesolow which caused the winds in this sounding to have a much stronger southerly component in the 850-400 hPa layer than in the sounding from the run using

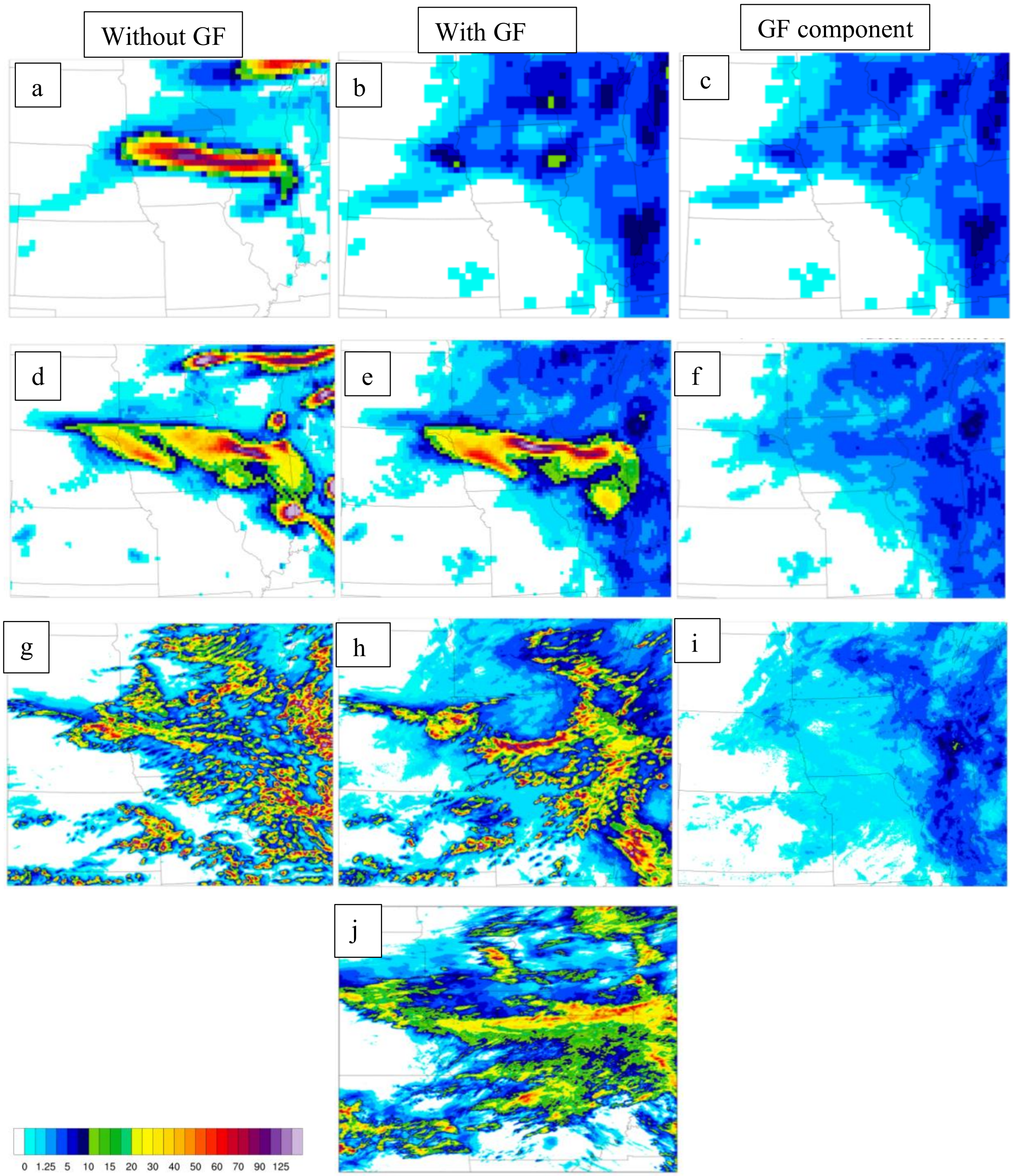

Figure 6: Total simulated rainfall (mm, see color bar at lower left) during the 0000 UTC 10 August – 0000 UTC 11 August period for the 25-km RRFS run a) without GF, b) with GF, and c) the convective component from GF, the 13-km RFFS run d) without GF, e) with GF, and f) the convective component from GF, and the 3-km RRFS run g) without GF, h) with GF, and i) the

convective component from GF. Observed precipitation from the Multi-Radar Multi-Sensor (MRMS) analysis is shown in j).

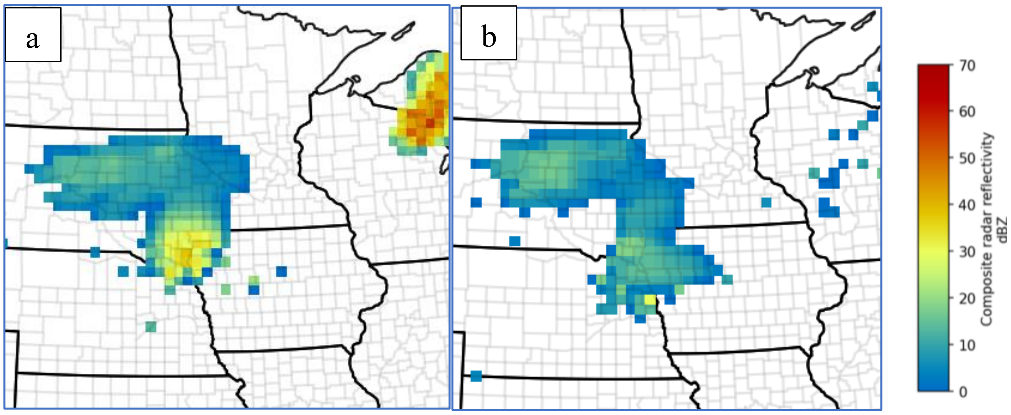

Figure 7: Simulated reflectivity at 1400 UTC 10 August 2020 for the simulations using RRFS physics a) without GF, and b) with GF.

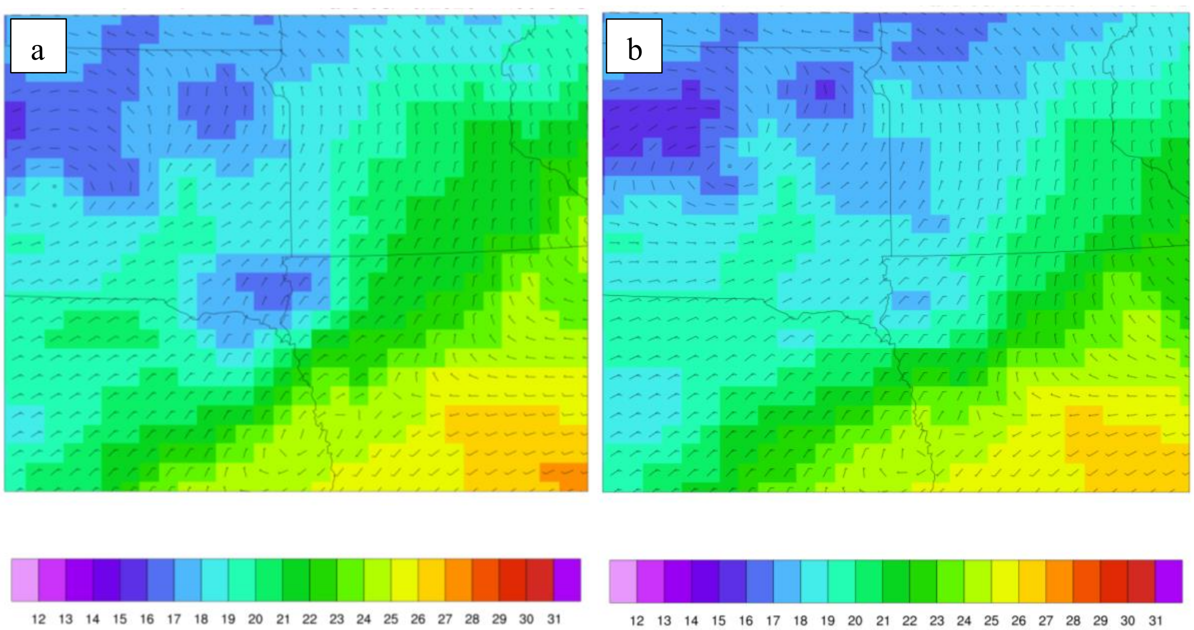

Figure 8: 2-m temperatures (˚C) at 1400 UTC 10 August 2020 for the 25 km runs using the RRFS physics a) without GF, and b) with GF.

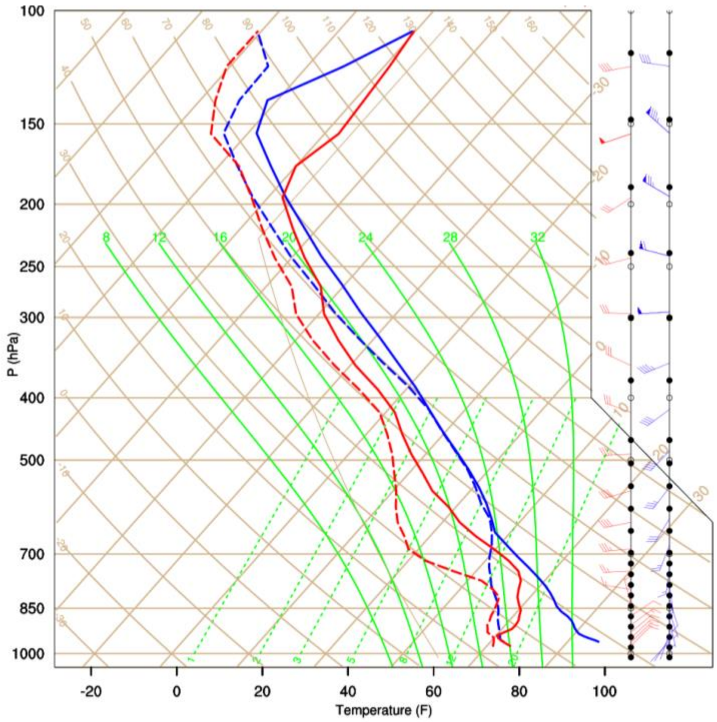

Figure 9: Comparison of soundings for a point at 42.5 N and 94.17 W in central Iowa (see Fig. 5b) at 1700 UTC in the 25-km runs using RRFS physics without the GF scheme (blue) and with the GF scheme (red).

GF. The use of the GF scheme greatly reduced the cold pool strength, so that there was insufficient lift to initiate grid-resolved precipitation, and thus only the weak reflectivity values associated with lighter precipitation due to the scheme were present.

For the 13-km runs, differences were much smaller between the runs without GF (Fig. 5c) and with GF (Fig. 5d), as would be expected with a scale-aware convective scheme. Both runs resembled observations well (Fig. 1b), showing a bowing echo in Iowa, although the run using GF had slightly more intense echo along the bowing segment. The amounts of precipitation produced by the GF scheme were similar in the 25-km (Fig. 6c) and 13-km (Fig. 6f) runs. However, whereas the activation of the GF scheme on the 25-km grid prevented the formation of substantial grid-resolved precipitation, the activation on the 13-km grid did not.

In the 3-km simulations, the differences were pronounced. The run not using GF (Fig. 5e) had its most organized convection in eastern IL arcing toward St. Louis, several hundred kilometers downstream of where the observed system was. This poor forecast was due to storms initiating during the prior evening and moving through Iowa during the night and early morning

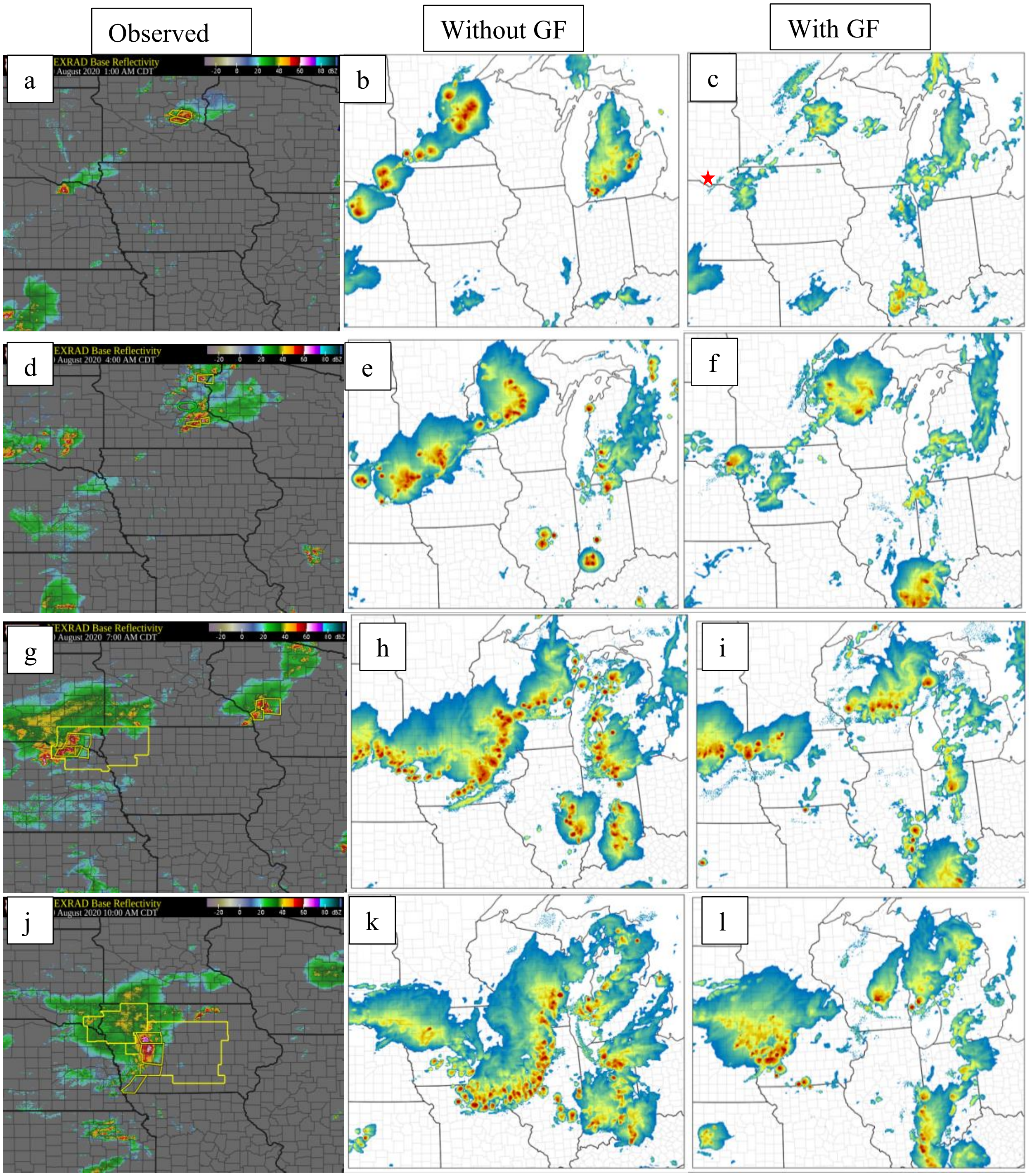
Observed
Without GF
With GF
a
b
c
d
e
f
g
h
i
j
k
l
EXRAD Base Reflectivity
August 2020 1:00 AM CDT
August 2020 4:00 AM CDT
August 2020 7:00 AM CDT
August 2020 10:00 AM CDT

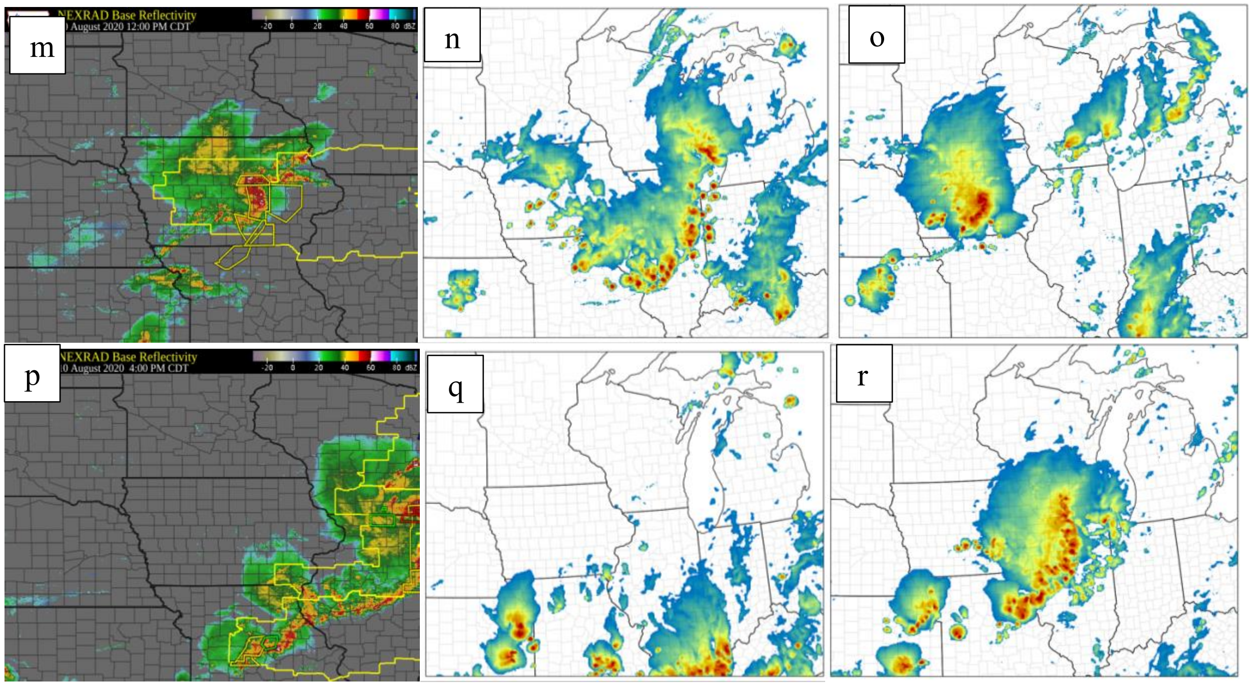

Figure 10: Observed reflectivity (left), and simulated reflectivity from the 3-km RRFS run without the GF scheme (middle column) and the RRFS run with the GF scheme (right column) at 0600 UTC (a-c), 0900 UTC (d-f), 1200 UTC (g-i), 1500 UTC (j-l) 1700 UTC (m-o), and 2100 UTC (p-r). Red star in panel c indicates where sounding used in Fig. 13 is taken.

(Fig. 10b, e, h). The development of spurious convection contrasts with the 3 km HRRRx run whose output provided the IC/LBCs for the FV3-LAM run (not shown). The HRRRx output was specifically used because it was one of the few operational or quasi-operational models to not develop much spurious convection during the night prior to the derecho (not shown). In the run with GF, the spurious nocturnal storms were replaced with some patches of light rain (Fig. 10c, f), and a stronger convective system was able to organize in roughly the correct parts of southeastern SD and eastern NE and move into western IA during the 1200-1500 UTC period (Fig. 10i, l). When the derecho was most intense, around 1700 UTC, the 3-km run with the GF scheme did show intense convection in southeastern Iowa (Fig. 10o), with just a small displacement error to the south (compare to Fig. 10m). The simulated system exhibited bowing at this time and grew upscale into a long arc by 2100 UTC (Fig. 10r), similar to what was observed (Fig. 10p) with just a small delay - less than an hour - in the simulated speed. Almost no simulated convection was present in the areas where it was observed from 1700-2100 UTC in the 3-km run that did not use GF (Fig. 10m and p compared to n and q).

The fact that the RRFS run with GF did not produce spurious strong storms during the previous night resulted in a very different forecast of precipitation in Iowa (compare Fig. 6g to Fig. 6h) with the run using GF (Fig. 6h) more correctly showing the concentrated swath of heavy rain in the path of the derecho. In that run, the convective scheme resulted in small areas of light rainfall (Fig. 6i) in the same general regions where spurious intense convection had happened in the run without GF. The role of spurious convection in preventing simulation of the derecho in many CAM simulations has been attributed to the removal of CAPE in these runs (personal communication, P. Skinner, CIMMS, E. Szoke, NOAA/GSL, J. Duda, NOAA/GSL). This is verified in the FV3-LAM runs by a comparison of the CAPE fields during the morning in Iowa when the derecho was organizing and intensifying (Fig. 11). The 3 km-run without GF had almost no CAPE in Iowa, whereas the 3-km run with GF had very high values at 1500 UTC, exceeding 3,000 J kg^{-1} in some areas. Differences in CAPE were much less among the runs with 13 and 25 km grid spacing, both with and without GF, and the fields were generally similar to the 3 km run that did use GF, although that run had a slightly smaller region of values over 3000 J kg^{-1}. Except for the 3 km run without GF, the simulated CAPE (Fig. 11f) agreed well with observations from the SPC mesonalyses from the morning of the event (Fig. 11g), although there was a negative bias of roughly 500 J kg^{-1} in the simulated values. The negative bias was due to simulated low-level temperatures and dew points generally being around 1°C too cool compared to observations in the pre-storm environment in Iowa (not shown).

Although the present study has focused on the runs using the RRFS physics suite, since this suite is currently planned for implementation into the version of the FV3-LAM that will be used operationally for high-resolution forecasting guidance, it was not just these RRFS runs that showed unusual behavior. In the runs using the GFS physics suite (with SAS convective parameterization), again the coarser 25- and 13-km grid spacing simulations performed much better than the one using 3 km horizontal grid spacing (Fig. 12). The same issue with spurious convection the previous night was present in the 3-km GFS run (not shown).

The results from the runs using the RRFS physics suite are unusual in that it is normally believed a convective parameterization is most needed for coarser resolutions and can be neglected for convection-allowing grid spacings. For this case, the coarsest runs (25 km grid spacing) had

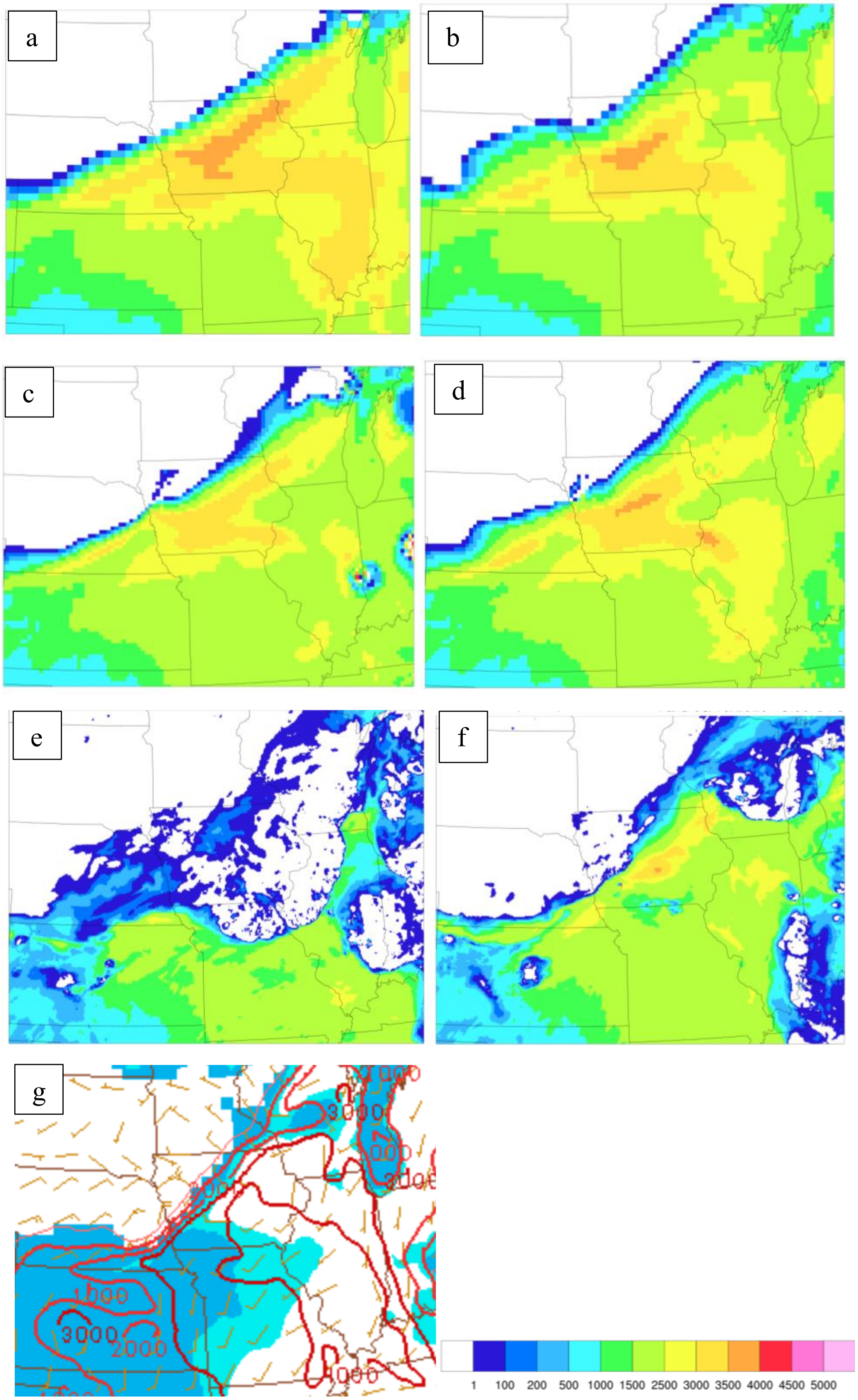
a
b
c
d
e
f
g
3000
1000
2000
1 100 200 500 1000 1500 2500 3000 3500 4000 4500 5000

Figure 11: Simulated surface-based CAPE at 1500 UTC for the RRFS runs initialized at 0000 UTC 10 August 2020 for a) 25 km without GF, b) 25 km with GF, c) 13 km without GF, d) 13 km with GF, e) 3 km without GF, and f) 3 km with GF. Values in J kg^{-1} indicated in a-f by color bar in lower right. The observed surface-based CAPE valid at this time (from SPC mesoanalysis archive) is shown in f with red contour intervals of 1000 J kg^{-1} with convective inhibition shaded (light blue 25 J kg^{-1} and darker blue 100 J kg^{-1}), and surface winds overlaid.

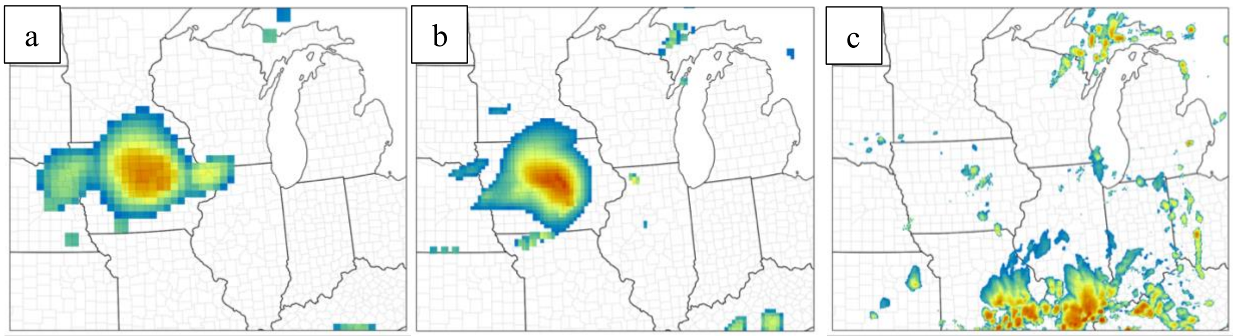

Figure 12: Simulated reflectivity at 1800 UTC for the GFS runs initialized at 0000 UTC with a) 25 km, b) 13 km, and c) 3 km horizontal grid spacing. The observed radar valid at this time can be found in Fig. 1b

worse forecasts when the GF scheme was used (Fig. 5b compared to Fig. 5a), while the finest run (3 km grid spacing) benefitted greatly from the use of the GF scheme. However, the benefit was not because the scheme was needed to trigger the event of interest but, instead, because the GF scheme prevented spurious convection from forming during the prior night (Fig. 10), which had resulted in poor depictions of the environment present during the morning when the derecho formed. The GF scheme only produced light rainfall amounts during the first few hours of the simulation, typically under 1 mm in most areas (as suggested in Fig. 6i), and although these rather broad regions were not supported by observations, the activation of the scheme led to a much better simulation of the later derecho.

An examination of surface-based CAPE and CIN during the hours around the time when the spurious convection formed (0400 and 0500 UTC) showed no noticeable differences between the runs with and without the GF scheme (not shown). However, a closer look at a sounding near where spurious convection formed in the run without GF showed that activation of the GF scheme warmed and dried a narrow layer just below 700 hPa in the general area where the spurious storms formed (Fig. 13). Such warming and drying with the GF scheme is due to compensating subsidence, and is often maximized at around 700 hPa (G. Grell, NOAA, 2023, personal communication). Although the impact may seem small at first glance, these changes have a large impact on the amount of lift needed to allow the elevated parcels that were experiencing the least CIN, such as at around 800 hPa, to rise to their level of free convection. The amount of lift needed to reach the level of free convection increased from around 50 hPa in the run that did not use GF to around 110 hPa in the run that did use GF.

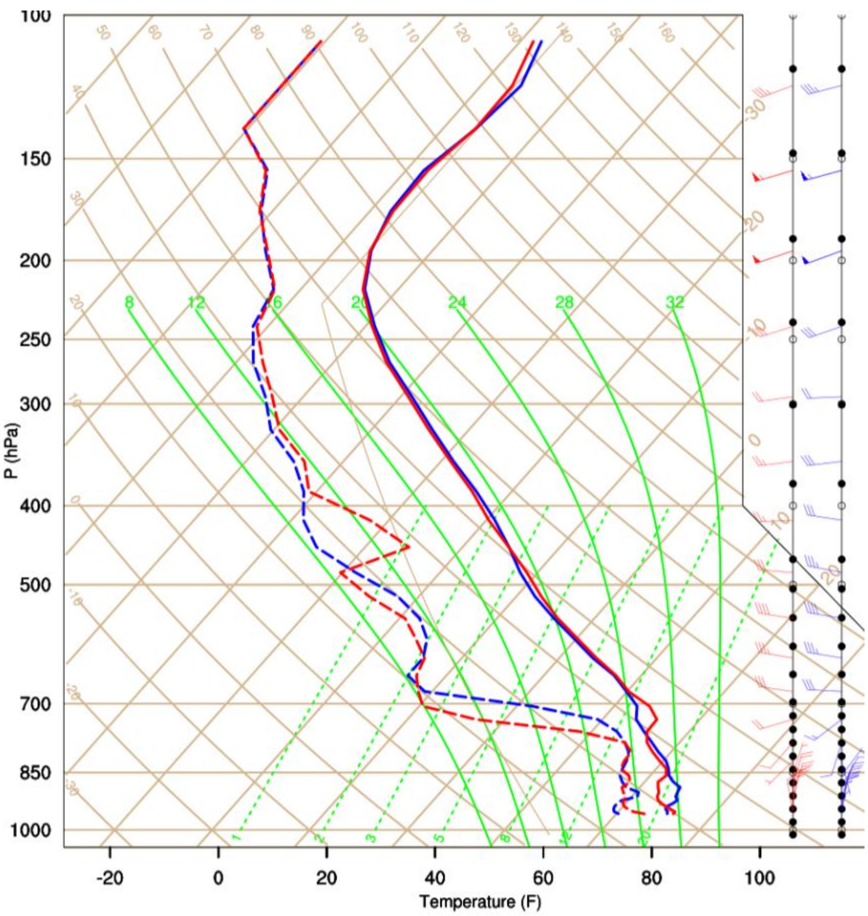

Figure 13: Soundings valid from a point in southeastern South Dakota (see Fig. 10c) near where spurious convection forms in the 3-km RRFS run not using the GF scheme, at 0400 UTC 10 August 2020 from the two 3-km runs with blue indicating the run without the GF scheme, and red the run with the GF scheme.

The simulated bow echo became extremely intense in this 3-km FV3-LAM run that used the GF scheme, producing an exceptionally strong cold pool and severe winds. At 1700 UTC, for instance, 2-m temperatures in the heart of the cold pool fell as low as 11° C, whereas the ambient temperatures ahead of the cold pool were around 28° C, so that a gradient of 17° C existed over about 50 km (Fig. 14). Observed temperatures reached 31° C in Cedar Rapids by 1600 UTC prior to the arrival of the derecho and fell as low as 14° C in Ames during the thunderstorms (surface data is limited during the event in Iowa as extensive power outages resulted in much data loss), implying the simulated intense cold pool was not an exaggeration. Sustained 10-m winds were simulated as high as 36 m s^{-1} at this time in and just northeast of the most northeastern cold pool temperature minimum in Fig. 14, and the gusts in the model (determined by mixing down momentum from the level of the top of the planetary boundary layer) approached 51 m s^{-1} (not shown). Sustained severe winds (25.7 m s^{-1} or more) covered an area over 20 km in length from west to east. An exceptional aspect of the observed derecho was the length of time over which severe winds occurred, reaching an hour or more in some locations near Cedar Rapids (Fowle et al. 2021). Thus, it is likely the coverage of strong winds is underestimated in this run.

Winds at 950 and 925 hPa at 1700 UTC, only about 250-500 m AGL, were as high as 60 m s^{-1} (see Fig. 15 for 950 hPa) with strong downward motion indicated in the region just behind and into the strongest winds. Fig. 15 shows a region corresponding to roughly the north half of the intense echo shown in Fig. 10o over south-central Iowa. Analysis of flow throughout the lowest few kilometers (not shown) revealed that a descending rear-inflow jet extended over 100 km in an arc moving counter-clockwise from a northerly direction becoming oriented primarily west to east where the strongest winds were located at 950 hPa, just behind the back of an arc of very strong upward motion associated with the bowing echo at this time (Fig. 15). Just to the northeast of the strongest winds, a circulation existed, associated with a strong mesolow where geopotential heights were over 100 m lower than just ahead of the storm. In the region with the peak height gradient associated with the mesolow, the change of 100 m occurred over a distance of only 15 km. The strongest winds in the simulation were confined to this region just southwest of the mesolow. The closed circulation was deep, extending upward to around 400 hPa (not shown), and winds of 40 m s^{-1} extended as far upward as 550 hPa. Radar did suggest a strong mesolow in the event, particularly around 1800 UTC just to the north of the strongest winds (at the north end of the bow echo shown in Fig. 1b). Rainfall of 75-100 mm occurred in a very narrow swath (Fig. 6h),

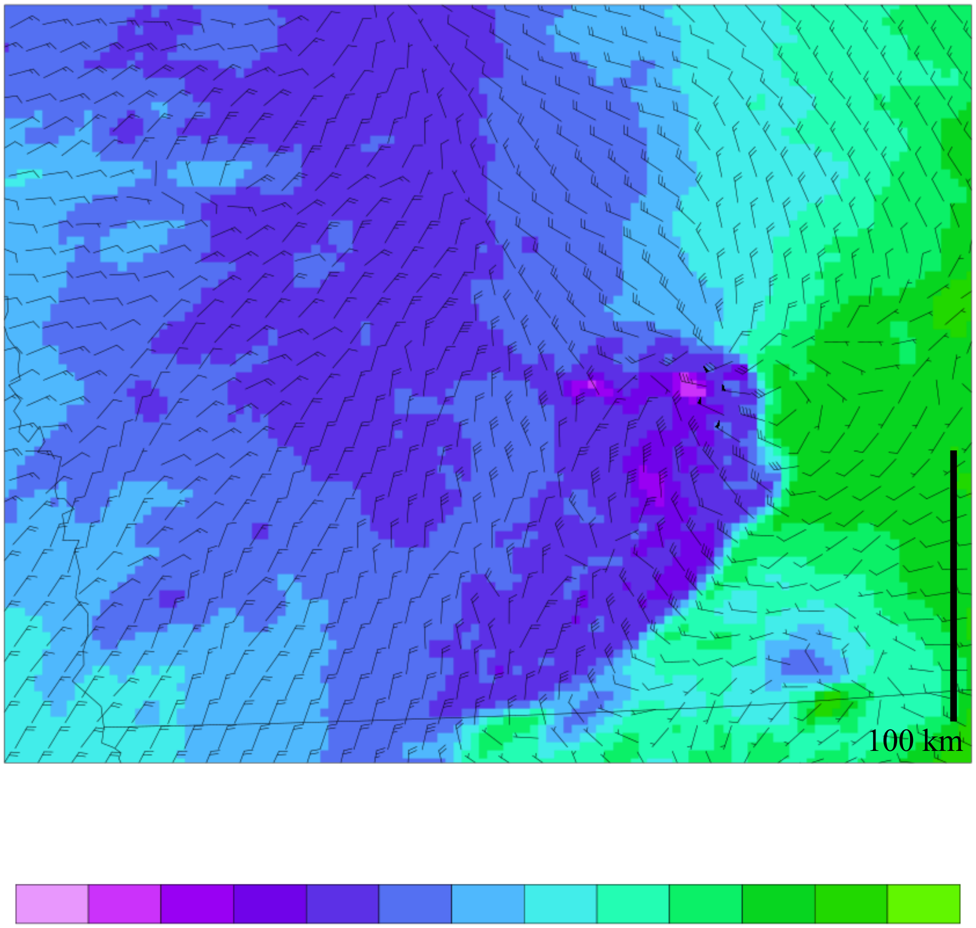

Figure 14: 2m temperatures (°C, see color bar below figure) and 10 m winds (barbs in knots) valid at 1700 UTC in the 3 km RRFS run using the GF scheme. Distance scale shown in lower right.

with much of the rain occurring in only an hour or less. The rainfall amounts were overestimated compared to observations (Fig. 6j) which showed peak values of 50-60 mm, but sustained winds of over 36 m s^{-1} were measured in many areas, with estimates based on damage as high as 63 m s^{-1}. Thus, the values being simulated by this FV3 run with 3 km horizontal grid spacing were in good agreement with what happened in this extreme event.

It is of some interest to compare the peak winds within the simulated strong convective system in Iowa when different horizontal grid spacings are used to understand how sensitive the winds are to changes in resolution, although it is likely operational forecasters would only be examining CAM output for guidance on severe convective hazards. The peak 10-m and 950-hPa winds simulated in the best-performing run using RRFS physics at each of the three horizontal grid spacings, while the convective system was most intense over Iowa during the period 1700 – 2000 UTC, is shown in Table 2. A pronounced increase in peak winds occurs as the grid spacing

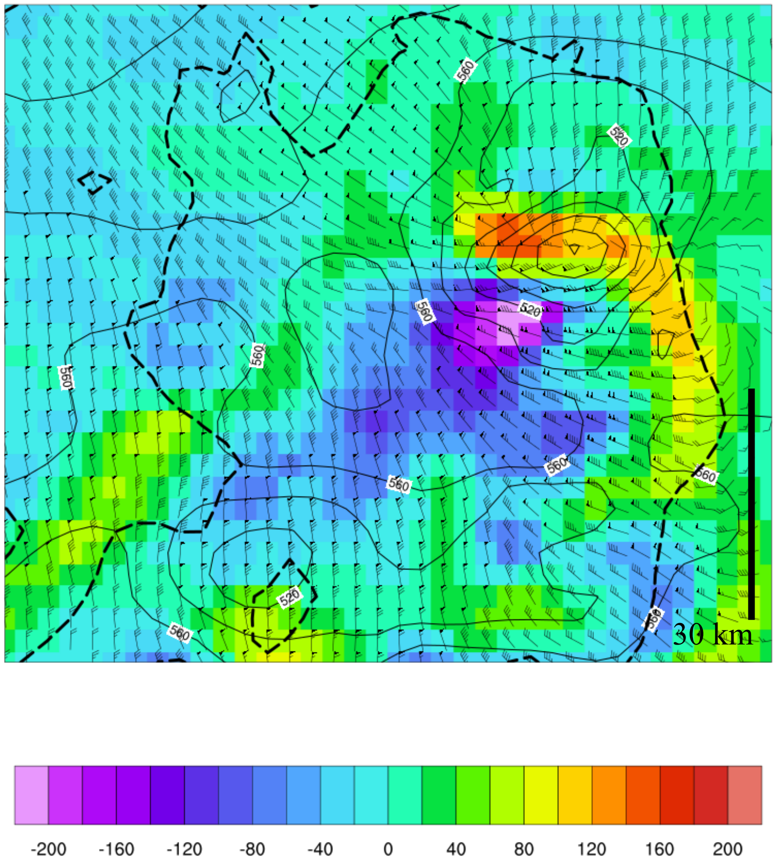

Figure 15: Vertical motion (cm s^{-1}, see color bar below figure), geopotential heights (black contours in m) and winds at 950 hPa (plotted every 3 km) over a portion of central Iowa at 1700 UTC in the 3-km RRFS run using the GF scheme. The 40-dBZ contour of simulated reflectivity is shown with a thick dashed black line. Distance scale shown in lower right.

Horizontal Grid Spacing (km)	Peak 10-m wind (m s^{-1})	Peak 950-hPa wind (m s^{-1})
25	23.5	29.4
13	31.6	59.7
3	41.8	64.6

Table 2: Peak sustained wind speed (based on instantaneous hourly values) during the period 1700 – 2000 UTC at 10 m and 950 hPa from the best-performing simulations using RRFS physics at 25, 13, and 3-km horizontal grid spacing. For the 25 km run, this was without GF, and for the 13 and 3 km runs, it was with GF.

is refined, although even with 13 km and 25 km grid spacing, the winds associated with the convective system were strong, with severe intensity at 10 m in the 13 km run, and at 950 hPa in the 25 km run, with 10-m winds just below the severe threshold.

5. Summary and Discussion

A very intense but poorly predicted derecho moved across portions of the United States Midwest on 10-11 August 2022. Damage exceeded 12 billion dollars. To gain understanding into why so many operational and quasi-operational runs, even with CAM horizontal grid spacings, failed to forecast the event when initialized less than 18 hours prior to its formation, a set of simulations was run using the FV3-LAM model with two different beta version physics suites (RRFS and GFS) and three different horizontal grid spacings. Simulations using the RRFS physics suite were also performed neglecting the use of the GF convective scheme at all three grid spacings.

Three unusual behaviors were discovered in the FV3-LAM runs. First, it was found that runs using the RRFS physics suite without the GF scheme correctly simulated an intense convective event in Iowa on 10 August in the coarse runs that used 13 and 25 km horizontal grid spacing, with relatively small spatial and temporal position errors around the time the derecho was most intense (1800 UTC). However, the finest grid spacing run, 3-km, failed to produce the derecho at all. Similar results were obtained when the GFS physics suite was used. This unusual behavior, with the finest grid performing by far the worst, was due to the development of spurious nocturnal convection in the 3-km runs, about 12 hours prior to the formation of the observed derecho. The late evening spurious storms grew upscale into a large MCS that rapidly removed nearly all instability across Iowa and parts of Illinois by the morning of 10 August, preventing more than some patches of light rain and isolated storms from being simulated on 10 August when the observed derecho was occurring. Observations showed no more than a few isolated storms happening the night before the 10 August derecho.

The second unusual finding with FV3-LAM is that when the GF convective scheme was turned on in the RRFS physics runs, the 25-km horizontal grid spacing results worsened substantially. The intense convective storms that had been produced in Iowa without the GF scheme were removed when GF was used, so that the only precipitation simulated during the time of the derecho was a steady rain area with moderate simulated reflectivity over southern Minnesota. In the 13-km simulation, use of the GF scheme had little impact on the simulation, which remained relatively accurate, with an even more pronounced bowing arc of intense reflectivity in central Iowa than in the run without GF around the time the observed derecho was in east-central Iowa.

The third unusual behavior was that the use of the GF scheme in the 3-km horizontal grid spacing run, a grid spacing where convective schemes are usually ignored, greatly improved the forecast. Instead of no organized convection in Iowa, the case when GF was not used, an unusually intense bowing line of convection was simulated with GF, with very small spatial and temporal displacement errors, significantly severe wind sustained at over 40 m s^{-1} with gusts over 51 m s^{-1}, and a very intense cold pool similar to that observed with a -17 °C temperature perturbation. The reason for the vast improvement in the forecast was not that the GF scheme played any role with the daytime derecho-producing convection but that it stopped the spurious storms that had happened the night before in the model run that did not use the GF scheme. The GF scheme activated in the first few hours of the forecast to produce some patches of light rainfall, and resulted in 1-2 °C of warming in a roughly 30-hPa-deep layer just below 700 hPa which effectively capped the atmosphere to the development of the spurious elevated nocturnal storms. Without the spurious convection, the run correctly showed a very unstable atmosphere across Iowa during the daytime of 10 August 2022, allowing a remarkably intense convective system to develop, similar in strength to what was observed.

These unusual behaviors raise some questions related to forecasting. Because so many operational models were unable to simulate the derecho, one might conclude that the event had poor predictability. However, the fact that both 13 and 25 km horizontal grid spacing runs were able to correctly show intense echo with small space and time errors, including the RRFS run that did not even use a convective scheme, suggests the event may have had high predictability, as long as the development of early spurious convection was suppressed. In a broader sense, problems with this spurious development likely involved errors in initial conditions, as evidenced by the fact that among operational and quasi-operational model runs initialized at 0000 UTC 10 August, only the HRRR run avoided the problem. In the present study, the use of the 0000 UTC HRRR output for initialization and lateral boundary conditions for the FV3-LAM avoided the problem in most runs, likely due to a more accurate depiction of the mesoscale environment at 0000 UTC, but the fact the 3-km run without GF still triggered spurious nocturnal storms shows how volatile the atmosphere was, with abundant elevated CAPE and minimal CIN, so that errors in depiction of vertical motion could still trigger the spurious convection.

The observation that the 25-km RRFS run worsened when the GF convective scheme was turned on is troubling. Further research should look at a broader sample of significant events to see how common this situation is, especially as the LAM version of the UFS prepares to become operational in 2024. For this case, it appears the environment supported development of an unusually strong cold pool, allowing the 25-km run without GF to trigger intense convection in a region where the scheme itself would only produce light rain. Finally, the success of the 3-km run that used GF raises several questions of its own, especially as CAM grid spacings are more commonly used for operational guidance. Does this result suggest that the GF scheme should always be used in the RRFS physics suite, even with a 3 km grid? In a larger sample of cases, would its primary role be in preventing spurious convection more so that helping with depiction of other storms? It must be noted, however, that even if a configuration like this (using a convective scheme) were used in a high-resolution ensemble, forecasters would still face the challenge that the probabilities for such an intense system would be low since most of the members, if not using a convective scheme, may fail to show a significant event. Perhaps the primary insight from the present study is that operational forecasters should pay close attention to model depictions of convection in the early periods of simulations and be aware that spurious convection early in a forecast may impact negatively the depiction of later convection. In the central United States, where nocturnal convection is common, close attention should be paid to the model forecasts in the first 12 hours for all 0000 UTC-initialized guidance.

Acknowledgments

This research was supported in part by National Science Foundation grant AGS2022888, and the Developmental Testbed Center. The DTC Visitor Program is funded by the National Oceanic and Atmospheric Administration, the National Center for Atmospheric Research and the National Science Foundation. The authors would like to thank Jeff Beck and Gerard Ketefian for their assistance with setting up the FV3-LAM experiments. The research benefitted from discussions with Edward Szoke, Jeff Duda, and Patrick Skinner from NOAA and Kathryn Newman at NCAR and DTC. Eric Aligo from NOAA kindly provided the 0000 UTC 10 August 2020 HREF member simulated reflectivity data, and Samuel Ritter at Iowa State created the plot of that data. Jonathan Thielen at Colorado State University provided the python codes for creation of the simulated reflectivity plots. We acknowledge the importance of open source Python code and packages (Matplotlib, NumPy, MetPy), which were used for some of the analysis in this study. The constructive comments of two reviewers are also acknowledged.

Data Availability Statement

The data that supports the findings of this work, including the HRRRx output used for initial and lateral boundary conditions, and the input files used to configure the nine FV3-LAM simulations, are stored on NCAR's campaign storage, and are available from the corresponding author upon request.

REFERENCES

Ashley, W. S., and T. L. Mote, 2005: Derecho hazards in the United States. Bull. Amer. Meteor. Soc., 86, 1577-1592.

Atkins, N. T., and M. St. Laurent, 2009: Bow echo mesovortices. Part I: Processes that influence their damaging potential. Mon. Wea. Rev., 137, 1497–1513.

Benjamin, S. G., Weygandt S. , Smirnova T. G. , Hu M. , Peckham S. E. , Brown J. M. , Brundage K. , and Manikin G. S. , 2009: Assimilation of radar reflectivity data using a diabatic digital filter: Applications to the Rapid Update Cycle and Rapid Refresh and initialization of High Resolution Rapid Refresh forecasts with RUC/RR grids. Preprints, 13th Conf. on Integrated Observing and Assimilation Systems for Atmosphere, Oceans, and Land Surface (IOAS-AOLS), Phoenix, AZ, Amer. Meteor. Soc., 7B.3. [Available online at https://ams.confex.com/ams/pdfpapers/150469.pdf.]

Benjamin, S. G., Weygandt S. , Alexander C. , Brown J. M. , Smirnova T. G. , Hofmann P. , James E. , and Dimego G. , 2011: NOAA's hourly-updated 3km HRRR and RUC/Rapid Refresh—Recent (2010) and upcoming changes toward improving weather guidance for air-traffic management. Proc. Second Aviation, Range, and Aerospace Meteorology Special Symp. on Weather–Air Traffic Management Integration, Seattle, WA, Amer. Meteor. Soc., 3.2. [Available online at https://ams.confex.com/ams/91Annual/webprogram/Paper185659.html.]

Benjamin, S. G., and Coauthors, 2013: Data assimilation and model updates in the 2013 Rapid Refresh (RAP) and High-Resolution Rapid Refresh (HRRR) analysis and forecast systems. NCEP/EMC Meeting, Washington, DC, NCEP/EMC/Model Evaluation Group. [Available online at http://ruc.noaa.gov/pdf/NCEP_HRRR_RAPv2_6jun2013-Benj-noglob.pdf.]

Bentley, M. L., and T. L. Mote, 1998: A climatology of derecho-producing mesoscale convective systems in the central and eastern United States, 1986-95. Part I: Temporal and spatial distribution. Bull. Amer. Meteor. Soc., 79, 2527-2540.

_______, and J. A. Sparks, 2003: A 15 yr climatology of derecho-producing mesoscale convective systems over the central and eastern United States. Climate Res., 24, 129-139

Black, T. L., J. A. Abeles, B. T. Blake, D. Jovic, E. Rogers, and X. Zhang, 2021: A limited area modeling capability for the Finite-Volume Cubed-Sphere (FV3) dynamical core and comparison with a global two-way nest. Journal of Advances in Modeling Earth Systems, 13, e2021MS002483. https://doi.org/10.1029/2021MS002483.

Bryan, G. H., and J. M. Fritsch, 2000: Moist Absolute Instability: The Sixth Static Stability State. Bulletin of the American Meteorological Society 81, 6, 1207-1230, https://doi.org/10.1175/1520-0477(2000)081<1287:MAITSS>2.3.CO;2.

Cohen, A. E., M. C. Coniglio, S. F. Corfidi, and S. J. Corfidi, 2007: Discrimination of mesoscale convective system environments using sounding observations. Wea. Forecasting, 22, 1045–1062, https://doi.org/10.1175/WAF1040.1.

Coniglio, M. C., and D. J. Stensrud, 2004: Interpreting the climatology of derechos. Wea. Forecasting, 19, 595-605.

______, and M. B. Richman, 2004: An observational study of derecho-producing convective systems. Wea. Forecasting, 19, 320-337.

______, S. F. Corfidi, and J. S. Kain, 2011: Environment and early evolution of the 8 May 2009 derecho-producing convective system. Mon. Wea. Rev., 139, 1083-1102.

Corfidi, S. F. M. C. Coniglio, A. E. Cohen, and C. M. Mead, 2016: A proposed revision to the definition of “derecho”. Bull. Amer. Meteor. Soc., 97(6), 935-950. https://www.jstor.org/stable/26243449.

Doswell, C. A., and J. S. Evans, 2003: Proximity sounding analysis for derechos and supercells: An assessment of similarities and differences. Atmos. Res., 67, 117-133.

Dowell, D. C., C. R. Alexander, E. P. James, S. S. Weygandt, S. G. Benjamin, G. S. Manikin, B. T. Blake, J. M. Brown, J. B. Olson, M. Hu, T. G. Smirnova, T. Ladwig, J. S. Kenyon, R. Ahmadov, D. D. Turner, J. D. Duda, and T. I. Alcott, 2022: The High-Resolution Rapid Refresh (HRRR): An Hourly Updating Convection-Allowing Forecast Model. Part I: Motivation and System Description, Weather and Forecasting, 37(8), 1371-1395. https://doi.org/10.1175/WAF-D-21-0151.1.

Ek, M. B., K. E. Mitchell, Y. Lin, E. Rogers, P. Grunmann, and V. Koren, 2003: Implementation of Noah land surface model advances in the National Centers for Environmental Prediction operational mesoscale Eta model. Journal of Geophysical Research, 108(D22), 8851. https://doi.org/10.1029/2002JD003296.

Evans, J. S., and C. A. Doswell III, 2001: Examination of derecho environments using proximity soundings. Wea. Forecasting, 16, 329-342.

Fowle, M., R. Wolf, B. Barjenbruch, and L. Carlaw, 2021: Major Weather Events and Impacts of 2020, Amer. Meteor. Soc., Boston, MA, 2021, 13.6.

Fujita, T. T., 1978: Manual of downburst identification for Project NIMROD. Satellite and Mesometeorology Research Paper 156, Dept. of Geophysical Sciences, University of Chicago, 104 pp.

Gallus, W. A., Jr., J. Correia, Jr., and I. Jankov, 2005: The 4 June 1999 derecho event: A particularly difficult challenge for numerical weather prediction. Wea. Forecasting, 20, 705-728.

Grell, G. A. and S. R. Freitas, 2014: A scale and aerosol aware stochastic convective parameterization for weather and air quality modeling. Atmospheric Chemistry and Physics, 14, 5233–5250. https://doi.org/10.5194/acp-14-5233-2014.

Grunzke, C. T. and C. Evans, 2017: Predictability and Dynamics of Warm-Core Mesoscale Vortex Formation with the 8 May 2009 "Super Derecho" Event. Mon. Wea. Rev., 145, 811-832. DOI:10.1175/MWR-D-16-0217.1

Han, J., W. Wang, Y. C. Kwon, S.-Y. Hong, V. Tallapragada, and F. Yang, 2017: Updates in the NCEP GFS cumulus convection schemes with scale and aerosol awareness. Weather and Forecasting, 32(5), 2005– 2017. https://doi.org/10.1175/waf-d-17-0046.1

_____, M. L. Witek, J. Teixeira, R. Sun, H.-L. Pan, J. K. Fletcher, and C. S. Bretherton, 2016: Implementation in the NCEP GFS of a Hybrid Eddy-Diffusivity Mass-Flux (EDMF) boundary layer parameterization with dissipative heating and modified stable boundary layer mixing. Weather and Forecasting, 31(1), 341– 352. https://doi.org/10.1175/waf-d-15-0053.1.

Harris, L. M., and S.-J. Lin, 2013: A two-way nested global-regional dynamical core on the cubed-sphere grid. Monthly Weather Review, 141(1), 283– 306. https://doi.org/10.1175/MWR-D-11-00201.1.

_____ and ______, 2014: Global-to-regional nested grid climate simulations in the GFDL high resolution atmospheric model. Journal of Climate, 27(13), 4890– 4910. https://doi.org/10.1175/Jcli-D-13-00596.1.

Heinzeller, D., Bernardet, L., Firl, G., Zhang, M., Sun, X., and Ek, M.: The Common Community Physics Package (CCPP) Framework v6, Geosci. Model Dev., 16, 2235–2259, https://doi.org/10.5194/gmd-16-2235-2023, 2023.

Hinrichs, G., 1888: Tornadoes and derechos. Amer. Meteor. J., 5, 341-349.

Iacono, M. J., J. S. Delamere, E. J. Mlawer, M. W. Shephard, S. A. Clough, and W. D. Collins, 2008: Radiative forcing by long-lived greenhouse gases: Calculations with the AER radiative transfer models. Journal of Geophysical Research, 113(D13), D13103. https://doi.org/10.1029/2008JD009944.

James, E. P., Alexander, C. R., Dowell, D. C., Weygandt, S. S., Benjamin, S. G., Manikin, G. S., Brown, J. M., Olson, J. B., Hu, M., Smirnova, T. G., Ladwig, T., Kenyon, J. S., and Turner, D. D., 2022: The High-Resolution Rapid Refresh (HRRR): An Hourly Updating Convection-Allowing Forecast Model. Part II: Forecast Performance. Weather and Forecasting 37, 8, 1397-1417, https://doi.org/10.1175/WAF-D-21-0130.1.

Janjic, Z. I., and R. L. Gall, 2012: Scienti ´ fic documentation of the NCEP nonhydrostatic multiscale model on the B grid (NMMB). Part 1: Dynamics. NCAR Tech. Note NCAR/TN4891STR, 75 pp., https://doi.org/10.5065/D6WH2MZX.

Johns, R. H. and W. D. Hirt, 1987: Derechos: Widespread convectively induced windstorms. Wea. Forecasting, 2, 32-49.

Kain, J. S., S. R. Dembek, S. J. Weiss, J. L. Case, J. J. Levit, and R. A. Sobash, 2010: Extracting unique information from high resolution forecast models: Monitoring selected fields and phenomena every time step. Wea. Forecasting, 25, 1536–1542, https://doi.org/10.1175/2010WAF2222430.1.

Lin, S.-J., 2004: A “Vertically Lagrangian” finite-volume dynamical core for global models. Monthly Weather Review, 132(10), 2293– 2307.

Long, P. J., 1986: An economical and compatible scheme for parameterizing the stable surface layer in the medium range forecast model (NCEP office note 321). Retrieved from https://www.ncep.noaa.gov/officenotes/NOAA-NPM-NCEPON-0004/01408602.pdf

______, 1989: Derivation and suggested method of the application of simplified relations for surface fluxes in the medium-range forecast model: Unstable case (NCEP office note 356). Retrieved from https://www.ncep.noaa.gov/officenotes/NOAA-NPM-NCEPON-0005/0140893E.pdf

Mahoney, K. M., and G. M. Lackmann, 2011: The sensitivity of momentum transport and severe surface winds to environmental moisture in idealized simulations of a mesoscale convective system. Mon. Wea. Rev., 139, 1352-1369. https://doi.org/10.1175/2010MWR3468.1.

Mlawer, E. J., S. J. Taubman, P. D. Brown, M. J. Iacono, and S. A. Clough, 1997: Radiative transfer for inhomogeneous atmospheres: RRTM, a validated correlated-k model for the longwave. Journal of Geophysical Research, 102(D14), 16663– 16682. https://doi.org/10.1029/97JD00237.

Nakanishi, M. and H. Niino, 2009: Development of an improved turbulence closure model for the atmospheric boundary layer. J. Meteor. Soc. Japan, 87, 895–912, doi:http://dx.doi.org/10.2151/jmsj.87.895.

Niu, G.-Y., et al. (2011), The community Noah land surface model with multiparameterization options (Noah-MP): 1. Model description and evaluation with local-scale measurements, *J. Geophys. Res.*, 116, D12109, doi:10.1029/2010JD015139.

NOAA National Centers for Environmental Information (NCEI) U.S. Billion-Dollar Weather and Climate Disasters (2022). https://www.ncei.noaa.gov/access/billions/, DOI: 10.25921/stkw-7w73

Olson, J. B., J. S. Kenyon, W. M. Angevine, J. M. Brown, M. Pagowski, and K. Sušelj, 2019: A description of the MYNN-EDMF scheme and coupling to other components in WRF-ARW. NOAA Tech. Memo. OAR GSD, 61, 37 pp., https://doi.org/10.25923/n9wm-be49.

______, T. Smirnova, J. S. Kenyon, D. D. Turner, J. M. Brown, W. Zheng, and B. W. Green, 2021: A description of the MYNN surface-layer scheme. NOAA Tech. Memo. OAR GSL-67, 26 pp., https://doi.org/10.25923/f6a8-bc75.

Putman, W. M. and S.-J. Lin, 2007: Finite-volume transport on various cubed-sphere grids. Journal of Computational Physics, 227(1), 55– 78. https://doi.org/10.1016/j.jcp.2007.07.022.

Ribeiro, B. Z., S. J. Weiss, and L. F. Bosart, 2022: An Analysis of the 3 May 2020 Low-Predictability Derecho Using a Convection-Allowing MPAS Ensemble. Wea. Forecasting, 37, 219–239, https://doi.org/10.1175/WAF-D-21-0092.1.

Rogers, E., and Coauthors, 2017: Upgrades to the NCEP North American Mesoscale (NAM) system. Bluebook Rep., 2 pp., http://wmc.meteoinfo.ru/bluebook/uploads/2017/docs/05_Rogers_Eric_mesoscale_modeling.pdf.

Rutledge, S. A., R. A. Houze, M. I. Biggerstaff, and T. Matejka, 1988: The Oklahoma–Kansas mesoscale convective system of 10–11 June 1985: Precipitation structure and single-Doppler radar analysis. Mon. Wea. Rev., 116, 1409–1430.

Skamarock, W. C., and Coauthors, 2008: A description of the Advanced Research WRF version 3. NCAR Tech. Note NCAR/TN-4751STR, 113 pp., https://doi.org/10.5065/D68S4MVH.

Thompson, G. and T. Eidhammer, 2014: A study of aerosol impacts on clouds and precipitation development in a large winter cyclone. Journal of the Atmospheric Sciences, 71(10), 3636--3658. https://doi.org/10.1175/JAS-D-13-0305.1.

Trapp, R. J., and M. L. Weisman, 2003: Low-level mesovortices within squall lines and bow echoes. Part II: Their genesis and implications. Mon. Wea. Rev., 131, 2804–2823.

Weisman, M. L., 1992: The role of convectively generated rear-inflow jets in the evolution of long-lived mesoconvective systems. J. Atmos. Sci., 49, 1826–1847.

______, 1993: The genesis of severe, long-lived bow echoes. /. Atmos. Sci., 50, 645-670.

——, and R. J. Trapp, 2003: Low-level mesovortices within squall lines and bow echoes. Part I: Overview and dependence on environmental shear. Mon. Wea. Rev., 131, 2779–2803.

_____, C. Evans, and L. Bosart, 2013: The 8 May 2009 Superderecho: Analysis of a Real-Time Explicit Convective Forecast. Wea. Forecasting, 28, 863–892, https://doi.org/10.1175/WAF-D-12-00023.1.

Zhou, L., S.-J. Lin, J.-H. Chen, L. M. Harris, X. Chen, and S. L. Rees, 2019: Toward convective-scale prediction within the next generation global prediction system. Bulletin of the American Meteorological Society, 100(7), 1225– 1243. https://doi.org/10.1175/BAMS-D-17-0246.1